JCI insight

RESEARCH ARTICLE

Requirement of Treg-intrinsic CTLA4/PKCη signaling pathway for suppressing tumor immunity

Christophe Pedros,[1] Ann J. Canonigo-Balancio,[1] Kok-Fai Kong,[1,2] and Amnon Altman[1]

[1]Division of Cell Biology, La Jolla Institute for Allergy and Immunology, La Jolla, California, USA.

[2]Pfizer Oncology Research & Development, La Jolla, California, USA.

The ability of Tregs to control the development of immune responses is essential for maintaining immune system homeostasis. However, Tregs also inhibit the development of efficient antitumor responses. Here, we explored the characteristics and mechanistic basis of the Treg-intrinsic CTLA4/PKCη signaling pathway that we recently found to be required for contact-dependent Treg-mediated suppression. We show that PKCη is required for the Treg-mediated suppression of tumor immunity in vivo. The presence of PKCη-deficient (*Prkch*$^{-/-}$) Tregs in the tumor microenvironment was associated with a significantly increased expression of the costimulatory molecule CD86 on intratumoral CD103^{+} DCs, enhanced priming of antigen-specific CD8^{+} T cells, and greater levels of effector cytokines produced by these cells. Similar to mouse Tregs, the GIT/PAK/PIX complex also operated downstream of CTLA4 and PKCη in human Tregs, and GIT2 knockdown in Tregs promoted antitumor immunity. Collectively, our data suggest that targeting the CTLA4/PKCη/GIT/PAK/PIX signaling pathway in Tregs could represent a novel immunotherapeutic strategy to alleviate the negative impact of Tregs on antitumor immune responses.

Introduction

The immune system plays an active role in determining the fate of precancerous lesions, the outgrowth of malignant tumors, and the response to therapeutic regimens (1). Emerging data have established that, in many cancers, a strong immune cell component, particularly an increased ratio of tumor-infiltrating effector T (Teff) cells to tumor-promoting Tregs, can serve as a predictive biomarker of an effective response to cancer therapies (2–6). During the past decade, immunotherapeutic strategies aimed at inhibiting Treg function and/or enhancing Teff cell responses have achieved a sustained long-term survival in approximately 20% of cancer patients and, hence, have revolutionarily altered the therapeutic landscape for cancer treatment (7, 8). Therapeutic approaches to deplete Tregs, reduce their recruitment to tumors, or inhibit their functions are under investigation in clinical trials (9), but specifically targeting the tumor-promoting Treg population remains a challenge. Therefore, a better understanding of Treg function and regulation in antitumor immunity, in conjunction with new immune target discovery efforts, will likely provide the next generation of immunotherapies with improved clinical outcomes and mitigated adverse effects.

Anti-CTLA4 antibodies represent the first approved therapeutic checkpoint blockade strategy in the clinic (10). CTLA4 plays a dominant role in controlling the immune system through various mechanisms. The engagement of CTLA4 expressed by activated Teff cells can limit their activation by competing with CD28 for binding of their shared ligands, CD80/86, expressed by antigen-presenting cells (APCs), thereby limiting the costimulatory signals (11). On the other hand, the constitutive expression of CTLA4 by Tregs is indispensable for their suppressive activities, as revealed by the fatal T cell–mediated autoimmune disease occurring in Treg-specific CTLA4-deficient mice (12). Treg-expressed CTLA4 interacts with CD80/86 expressed by APCs and physically removes those ligands from the APC cell surface by transendocytosis, thereby limiting the ability of APCs to induce immune responses (13).

Despite the clinical success of anti-CTLA4 mAb, treatment with anti-CTLA4 mAbs often leads to the development of autoimmune-related adverse events that predominantly affect the skin and the gastrointestinal tract (14). Hence, identifying more specific and efficient strategies aimed at neutralizing the protumor

Conflict of interest: The authors have declared that no conflict of interest exists.

Submitted: June 13, 2017
Accepted: November 1, 2017
Published: December 7, 2017

Reference information:
JCI Insight. 2017;2(23):e95692.
https://doi.org/10.1172/jci.insight.95692.

functions of Tregs, while preserving their essential ability to maintain immune system homeostasis, is much needed. We recently reported that protein kinase C-η (PKCη) interacts with CTLA4 in Tregs and inducibly recruits a complex consisting of the PAK, PIX, and GIT proteins (15), which have been shown to control focal adhesion disassembly in non–T cells (16, 17). Furthermore, activation of this complex was defective in PKCη-deficient (*Prkch*$^{-/-}$) Tregs, likely resulting in impaired ability of Tregs to dissociate from engaged APCs and serially engage new APCs and inhibit their antigen-presenting function via depletion of costimulatory ligands, CD80 and/or CD86 (15). These events were important for Treg ability to control antitumor immune response against the murine B16 melanoma; however, PKCη was dispensable for the control of experimental autoimmune colitis (15). This dichotomy likely reflected the heterogeneity of Treg suppressive mechanisms and a selective impairment of contact-dependent suppressive mechanism(s) in *Prkch*$^{-/-}$ Tregs.

Using two syngeneic mouse tumor models, we here demonstrate that *Prkch*$^{-/-}$ Tregs were unable to promote the growth of TRAMP-C1 prostate cancer and B16 melanoma, thereby demonstrating the broad relevance of this pathway in tumor immunity. Analysis of the cellular mechanisms in the tumor microenvironment (TME) revealed that PKCη deletion from Tregs dampened their contact-dependent suppressive function in vivo by reducing their ability to deplete CD86 from DCs and, thereby, inhibit the costimulatory potential of intratumoral DCs. Consequently, tumor antigen-specific CD8$^+$ T cells were primed more efficiently in the presence of *Prkch*$^{-/-}$ Tregs, resulting in stronger Teff cell responses manifested by reduced tumor growth. We also demonstrate for the first time to our knowledge that PKCη interacts with CTLA4 in human Tregs and is required for their suppressive activity. Finally, GIT2 deficiency reduced the suppression of antitumor immunity by murine Tregs in vivo and knockdown of GIT2 expression impaired the suppressive activity of human Tregs in vitro, implicating GIT2 as a major molecular player that controls Treg-suppressive function downstream of the CTLA4/PKCη pathway. Targeting the CTLA4/PKCη/GIT/PAK/PIX signaling pathway might therefore represent a novel immunotherapeutic strategy to promote antitumor immunity while potentially preserving the ability of Tregs to maintain immune system homeostasis.

Results

The CTLA4/PKCη pathway controls human Treg-suppressive activity. We have previously established that a physical interaction exists between CTLA4 and PKCη in mouse Tregs (15). To explore the role of PKCη in human Tregs, we purified CD4$^+$CD25^{bright}CD127^{lo} T cells from the peripheral blood mononuclear cells (PBMCs) of healthy donors, resulting in a population of approximately 80% Foxp3$^+$ cells (data not shown). Sorted Tregs were left unstimulated or stimulated with anti-CD3 and anti-CTLA4 antibodies, and CTLA4 was immunoprecipitated. Blotting with an anti-PKCη antibody revealed minimal interaction between CTLA4 and PKCη in unstimulated Tregs, but this interaction was greatly induced in the stimulated cells (Figure 1A), demonstrating a physical, inducible interaction between PKCη and CTLA4 in primary human Tregs. To determine whether PKCη is required for the suppressive activity of human Tregs, we depleted PKCη using a lentiviral vector expressing an shRNA that targets *PRKCH* or a control shRNA. We achieved an 80%–95% knockdown efficiency of PKCη protein level (Figure 1, B and C) without affecting the level of Foxp3 protein in human Tregs (Figure 1D). The transduced Tregs were cocultured at different ratios with allogeneic CellTrace Violet– prelabeled (CTV-prelabeled) PBMCs in anti-CD3–coated plates, and proliferation of gated CD4$^+$ T cells was measured 4 days later by CTV dilution. When compared with Tregs transduced with control shRNA, knockdown of *PRKCH* using two different shRNA sequences significantly reduced the suppressive activity of the human Tregs in a dose-dependent manner (Figure 1, E and F). These data demonstrate that PKCη physically interacts with CTLA4 in human Tregs and that optimal in vitro suppressive activity of human Tregs depends on PKCη.

Tumor burden is reduced and intratumoral Teff cell accumulation is increased in the presence of Prkch$^{-/-}$ *Tregs*. To determine whether PKCη is required for the ability of Tregs to control antitumor immune responses in vivo, we adoptively transferred WT CD25-depleted splenocytes, a source of Teff cells, in the absence or presence of WT or *Prkch*$^{-/-}$ Foxp3-IRES-GFP (FIG) Tregs into *Rag1*$^{-/-}$ recipients and inoculated them 1 day later intradermally (i.d.) with the B16-F10 melanoma. Transfer of CD25-depleted splenocytes alone resulted in some tumor growth and the presence of WT Tregs significantly increased tumor burden, reflecting their ability to inhibit the development of antitumor immune responses (Figure 2A and Supplemental Figure 1; supplemental material available online with this article; https://doi.org/10.1172/jci.insight.95692DS1). In

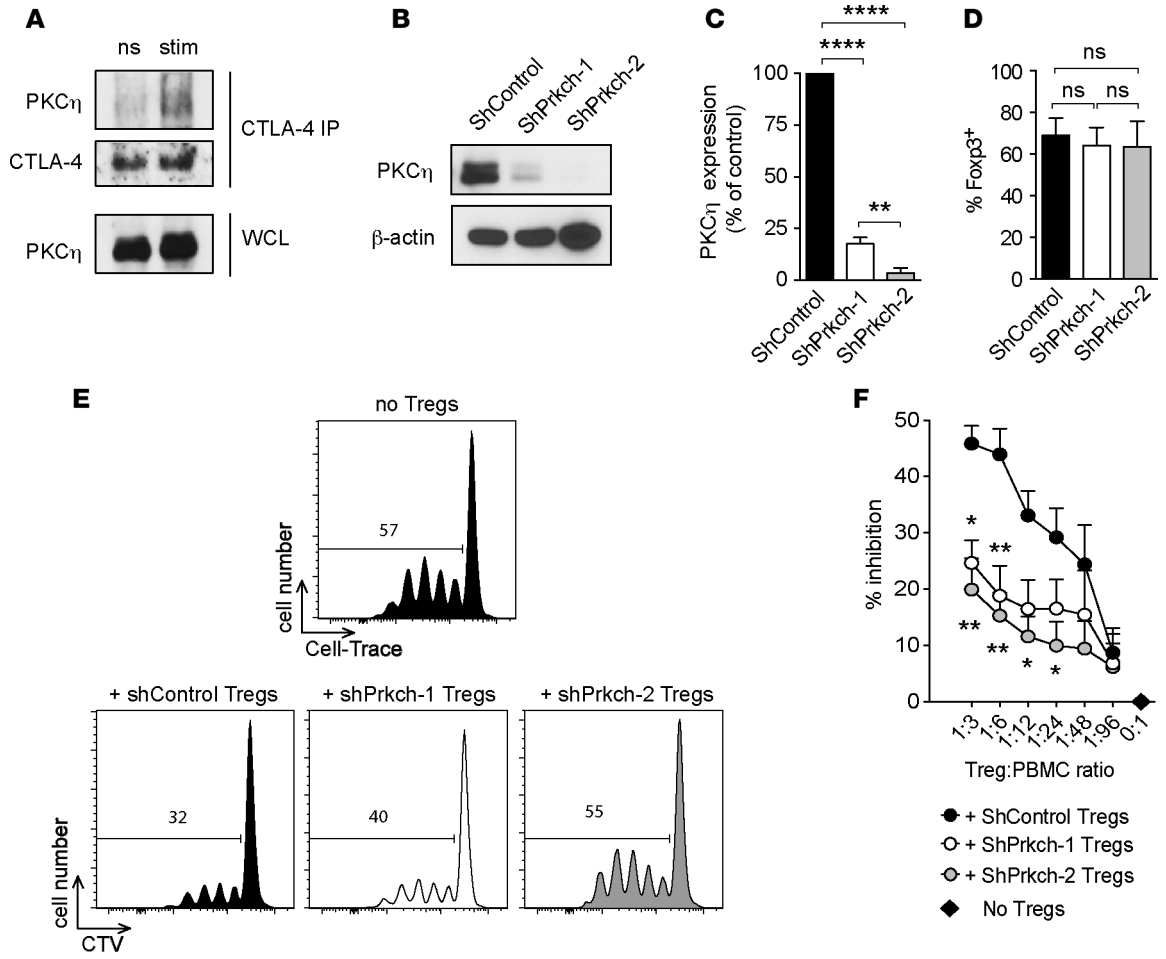

Figure 1. The CTLA4/PKCη pathway controls human Treg-suppressive activity. (**A**) $CD4^+CD25^+CD127^{lo}$ Tregs from human blood were left unstimulated (ns) or were stimulated (stim) for 5 minutes with anti-CD3 and anti-CTLA4 antibodies. CTLA4 immunoprecipitates and whole cell lysates (WCL) were immunoblotted with anti-PKCη and anti-CTLA4 antibodies. Data representative of 2 independent experiments are shown. (**B–D**) Human Tregs were retrovirally transduced with irrelevant shRNA (ShControl) or 2 different shRNA targeting *Prkch* (shPrkch-1 and shPrkch-2). PKCη expression in purified transduced Tregs was assessed by immunoblotting (**B**) and quantitated as the percentage of expression in the ShControl group (**C**). Foxp3 expression in transduced Tregs was assessed by intracellular staining (**D**). (**E** and **F**) Suppressive activity of the transduced Tregs was analyzed by coculture at different ratios with CTV-prelabeled PBMCs stimulated with anti-CD3. (**E**) Representative histograms of CTV dilution in gated $CD4^+$ responder cells. (**F**) Cumulative data expressed as the percentage inhibition of responder $CD4^+$ cell proliferation (mean ± SEM of 5 independent experiments). Statistical significance of differences between groups was determined by 1-way ANOVA and Tukey's multiple comparisons test. ns, $P > 0.05$; $^*P \le 0.05$; $^{**}P \le 0.01$; $^{****}P \le 0.0001$. Statistical significance levels are shown against the + ShControl Treg group.

contrast, *Prkch*$^{-/-}$ Tregs failed to enhance tumor growth, resulting in tumor sizes comparable to those mice that did not receive any Tregs. We observed similar results using a second syngeneic mouse tumor model, the slow growing, hormone-dependent TRAMP-C1 prostate adenocarcinoma (Supplemental Figure 2A).

Analysis of the TME in the B16-F10 model revealed a robust tumor infiltration of $CD4^+$ and $CD8^+$ T cells in *Rag1*$^{-/-}$ mice that received CD25-depleted splenocytes alone (Figure 2, B and C). As expected, the numbers of tumor-infiltrating $CD4^+$ and $CD8^+$ Teff cells were significantly reduced in the presence of WT Tregs. In contrast, *Prkch*$^{-/-}$ Tregs did not impede the accumulation of $CD4^+$ and $CD8^+$ Teff cell populations in the TME relative to mice that received no Tregs, indicating that *Prkch*$^{-/-}$ Tregs were unable to inhibit the development of antitumor immune responses (Figure 2, B and C). Although the difference in infiltrating $CD4^+$ T cell numbers between recipients of WT and *Prkch*$^{-/-}$ Tregs was not statistically significant, there was a clear tendency toward increased cell numbers in the presence of *Prkch*$^{-/-}$ Tregs (Figure 2C). Interestingly, the loss of PKCη was not associated with a reduced number of intratumoral Tregs (Figure 2D), largely ruling out the possibility of intratumoral homing and/or expansion defects in *Prkch*$^{-/-}$ Tregs. Of note, the CD8/Treg cell ratio was not significantly higher in the presence of *Prkch*$^{-/-}$ Tregs in the B16 model

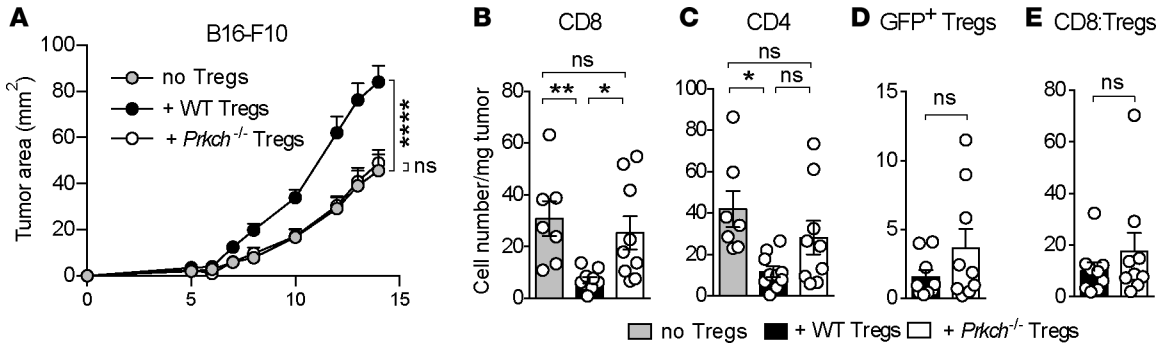

Figure 2. The presence of *Prkch*$^{-/-}$ Tregs reduces tumor growth and increases intratumoral Teff cell accumulation. *Rag1*$^{-/-}$ mice received CD25-depleted C57BL/6 spleen cells as a source of Teff cells either alone (no Tregs, gray) or together with CD4$^+$GFP$^+$ Tregs from WT (black) or *Prkch*$^{-/-}$ (white) FIG mice. B16-F10 melanoma cells (0.5×10^6) were inoculated i.d. 1 day later. (**A**) Tumor sizes were measured 3 times a week to calculate tumor area (mm^2), and cumulative data of 3–4 experiments are shown (mean ± SEM). no Tregs, $n = 16$; + WT Tregs, $n = 14$; + *Prkch*$^{-/-}$ Tregs, $n = 16$. (**B–E**) Numbers of tumor-infiltrating CD8$^+$ Teff (**B**), CD4$^+$ Teff (**C**), and GFP$^+$ Tregs (**D**) per mg of tumor and CD8/Treg ratios (**E**) were analyzed in B16-F10 tumors on day 14. Cumulative data of 3 experiments are shown (mean ± SEM). no Tregs, $n = 7$; + WT Tregs, $n = 10$; + *Prkch*$^{-/-}$ Tregs, $n = 9$. Statistical significance of differences between groups was determined by repeated-measures 2-way ANOVA (**A**) or 1-way ANOVA (**B–E**) followed by Tukey's multiple comparisons test. ns, $P > 0.05$; *$P \le 0.05$; **$P \le 0.01$; ****$P \le 0.0001$. Statistical significance levels in **A** are shown against the no Tregs group.

(Figure 2E), reflecting the slight but nonsignificant increase in tumor-infiltrating *Prkch*$^{-/-}$ Tregs (Figure 2D). Similar analysis of the TME in the TRAMP-C1 tumor model (Supplemental Figure 2, B–E) revealed a trend toward a reduction of the number of CD8$^+$ tumor-infiltrating lymphocytes (TILs) in the presence of WT Tregs, which was not significant, but not in the presence of *Prkch*$^{-/-}$ Tregs. Equivalent infiltration of TRAMP-C1 tumors by WT and *Prkch*$^{-/-}$ Tregs was observed (Supplemental Figure 2D), and, as a result, CD8/Treg ratios were increased in the presence of *Prkch*$^{-/-}$ Tregs (Supplemental Figure 2E), indicative of a TME more favorable for antitumor immunity and correlating with the improved tumor control (Supplemental Figure 2A). Altogether, these results show that PKCη expressed by Tregs is critical for their ability to inhibit the development of antitumor Teff cell responses. Importantly, the reduced tumor growth in the presence of *Prkch*$^{-/-}$ Tregs reflected the importance of CD8$^+$ Teff cells in controlling tumor growth, as the reduced tumor growth under this condition was reversed when CD8$^+$ T cells were depleted from the transferred spleen cells used as a Teff cell source (Supplemental Figure 3).

We also analyzed myeloid cell subsets present in the TME. The numbers of tumor-infiltrating CD11c$^+$MHC-II$^+$ DCs, CD11b$^+$F480$^+$ macrophages, and CD11b$^+$Gr1$^+$ myeloid-derived suppressor cells were not affected in the absence or presence of WT or *Prkch*$^{-/-}$ Tregs (Supplemental Figure 4).

Effector functions of intratumoral CD8$^+$ T cells are enhanced in the presence of Prkch$^{-/-}$ Tregs independent of PD-1 and Tim3. To further investigate the relevant cellular mechanisms, we analyzed the production of proinflammatory cytokines and the expression of exhaustion markers, including PD-1 and Tim3, by CD8$^+$ TILs. TILs were briefly stimulated ex vivo to analyze the production of IFN-γ, which is known to induce robust Teff cell antitumor responses and/or TNF-α. In *Rag1*$^{-/-}$ mice receiving CD25-depleted splenocytes but no Tregs, an average of approximately 30%, approximately 13%, and approximately 9% of the CD8$^+$ TILs expressed IFN-γ$^+$, TNF-α$^+$, or both cytokines simultaneously, respectively (Figure 3, A–D), representing the CTL response. The percentages of all these CTL populations were significantly diminished in the presence of WT Tregs but were unaffected in the presence of *Prkch*$^{-/-}$ Tregs (Figure 3, A–D). Similar results were observed for the IFN-γ$^+$ and the TNF-α$^+$CD4$^+$ TIL population (Supplemental Figure 5), albeit with a lower significance level. Taken together, these results reveal that, in the presence of *Prkch*$^{-/-}$ Tregs, tumors were not only infiltrated by increased numbers of Teff cells, but the infiltrating TILs also displayed enhanced effector function.

Exhaustion is a hallmark of dysfunctional CD8$^+$ T cells in the TME (18–20). As Tregs might promote the development of exhaustion through diverse and ill-defined mechanisms (21, 22), we questioned whether the enhanced TIL function observed in the presence of *Prkch*$^{-/-}$ Tregs relative to WT Tregs is associated with reduced expression of exhaustion markers, i.e., PD-1 and Tim3. In the absence of Tregs, we observed a substantial (~35%) population of CD8$^+$ T cells expressing PD-1 (Figure 3, E and F) and smaller subsets (~3%–5%) of Tim3$^+$ (Figure 3, E and G) or PD-1$^+$Tim3$^+$ (Figure 3, E and H) cells, the latter considered to be the most exhausted TIL population (19, 23). Intriguingly, the proportions of PD-1$^+$, Tim3$^+$, or double-positive (PD-1$^+$Tim3$^+$) CD8$^+$ TILs were not significantly elevated in the presence of *Prkch*$^{-/-}$ Tregs relative to WT

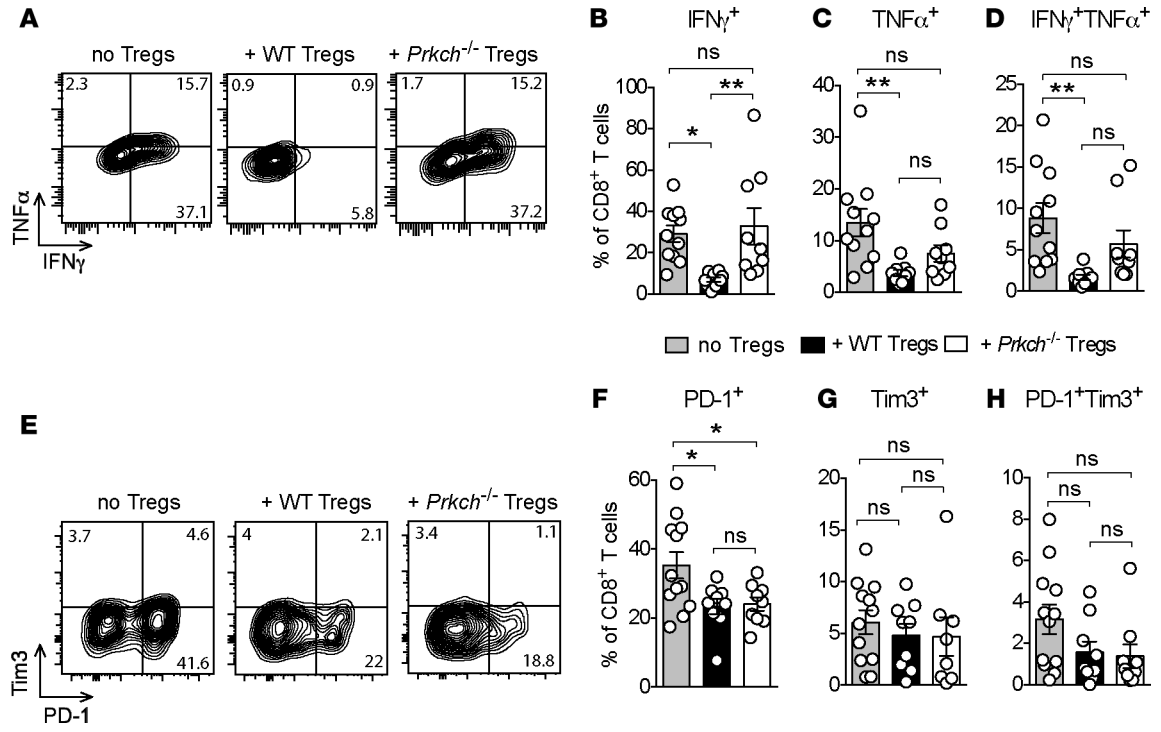

Figure 3. Increased effector cytokine production by CD8⁺ TILs in the presence of *Prkch*$^{-/-}$ Tregs. *Rag1*$^{-/-}$ mice received an adoptive transfer of CD25-depleted spleen cells with or without Tregs from WT or *Prkch*$^{-/-}$ FIG mice and were implanted with B16-F10 melanoma cells, as in Figure 2. (**A–D**) CD8⁺ TILs were harvested on day 14 and briefly stimulated ex vivo with PMA plus ionomycin to assess production of IFN-γ and TNF-α by intracellular staining. Representative dot plots of 1 mouse from each group (**A**) and percentage of IFN-γ⁺ (**B**), TNF-α⁺ (**C**), or IFN-γ⁺TNF-α⁺ (**D**) CD8⁺ TILs are shown. Cumulative data of 3 experiments (no Tregs, $n = 12$; + WT Tregs, $n = 9$; + *Prkch*$^{-/-}$ Tregs, $n = 9$). ns, $P > 0.05$; *$P \le 0.05$, **$P \le 0.01$. Statistical significance of differences between groups was determined by 1-way ANOVA and Tukey's multiple comparisons test. (**E–H**) Expression of PD-1 and Tim3 by CD8⁺ TILs was analyzed on day 14, showing dot plots of 1 representative mouse (**E**) and the percentage of PD-1⁺ (**F**), Tim3⁺ (**G**), or PD-1⁺Tim3⁺ (**H**) TILs.

Tregs (Figure 3, F–H), implying that under these conditions CD8⁺ TIL exhaustion does not play a major role in the failure of *Prkch*$^{-/-}$ Tregs to inhibit the effector function of these TILs and, hence, antitumor immunity. This result likely reflects the very low fraction of PD-1⁺Tim3⁺ cells (~2%–3%), which would not be expected to have much of an effect on the effector function of the TILs.

Increased priming of tumor antigen-specific T cells and intratumoral DC activation in the presence of Prkch$^{-/-}$ *Tregs.* Since T cell exhaustion did not seem to have a major effect on the defective suppression displayed by *Prkch*$^{-/-}$ Tregs, we asked whether *Prkch*$^{-/-}$ Tregs could modulate the priming of antigen-specific Teff cells. To probe antigen-specific CD8⁺ T cell priming in vivo, we inoculated ovalbumin-expressing B16 melanoma (B16-OVA) tumors i.d. into adoptive transfer *Rag1*$^{-/-}$ recipients of CD25-depleted splenocytes in the absence or presence of WT or *Prkch*$^{-/-}$ Tregs (Figure 4A). Ten days later, congenically marked (CD45.1⁺), CTV-labeled naive OT-I TCR-transgenic CD8⁺ T cells specific for the OVA peptide ^{257}SIINFEKL^{264} presented by H-2K^{b} were adoptively transferred i.v. into the tumor-bearing mice. The proliferation of these antigen-specific T cells infiltrating the tumors was analyzed 3 days after transfer. In *Rag1*$^{-/-}$ mice that received CD25-depleted splenocytes but no Tregs, we observed CTV dilution in approximately 32% of the transferred OT-I T cells (Figure 4B), indicating that these cells were effectively primed and proliferated within the TME. The in vivo proliferation of OT-I T cells was significantly reduced (9%) in the presence of WT Tregs, and the presence of *Prkch*$^{-/-}$ Tregs reduced the in vivo proliferation of intratumoral OT-I CD8⁺ T cells to an intermediate level of 19% (Figure 4, B and C). Although the difference in OT-I T cell proliferation in the presence of WT versus *Prkch*$^{-/-}$ Tregs did not reach significance when analyzed by 1-way ANOVA (Figure 4C), analysis by an unpaired *t* test revealed a significant difference ($P = 0.042$; data not shown). These results suggest that PKCη deficiency reduces the ability of Tregs to suppress the priming and proliferation of antigen-specific CD8⁺ TILs.

APCs in the TME play a key role in the initiation of antitumor responses (24, 25), and we previously reported that *Prkch*$^{-/-}$ Tregs exhibit a defective contact-dependent suppressive function in vitro,

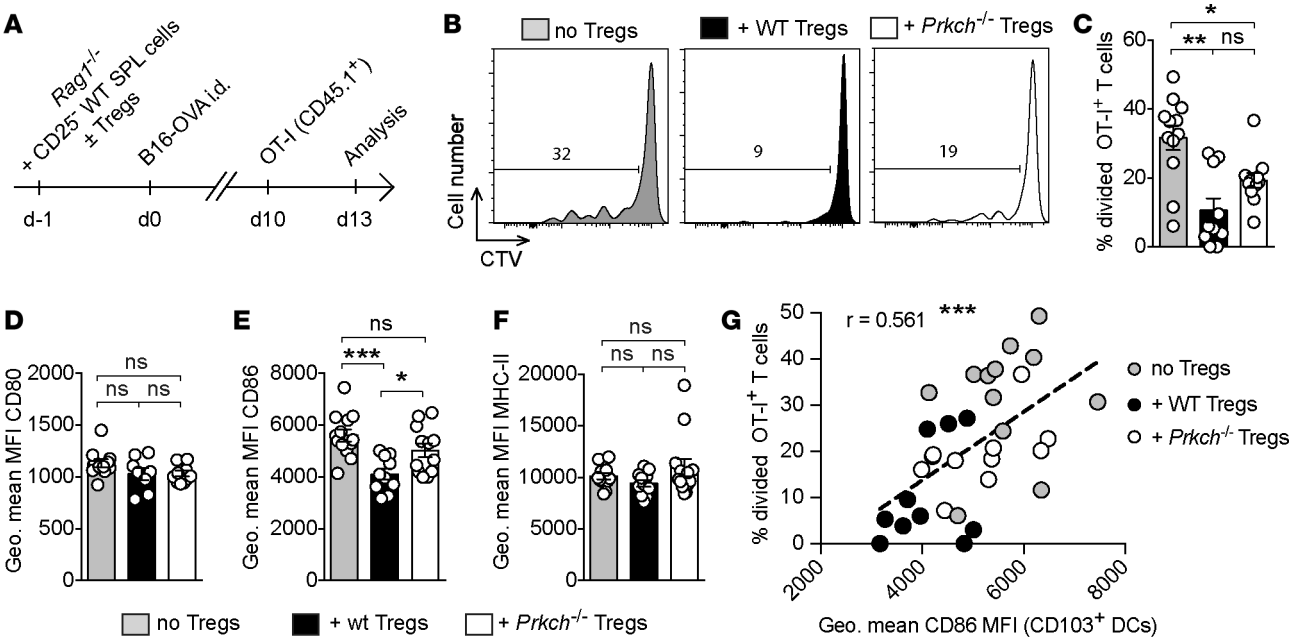

Figure 4. Increased priming of tumor antigen-specific T cells and CD103⁺ intratumoral DC activation in the presence of *Prkch*$^{-/-}$ Tregs. (**A**–**C**) *Rag1*$^{-/-}$ mice received an adoptive transfer of CD25-depleted spleen cells with or without Tregs from WT or *Prkch*$^{-/-}$ FIG mice and were implanted with OVA-expressing B16-F10 melanoma cells (B16-OVA), as in Figure 2. CTV-labeled naive OT-I CD8⁺CD45.1⁺ T cells were transferred i.v. into tumor-bearing mice on day 10. (**A**) The in vivo proliferation of intratumoral OT-I CD8⁺ T cells was assessed 3 days after transfer. Representative CTV dilution histograms (**B**) and the percentage of divided OT-I CD8⁺ T cells (**C**) are shown. (**D**–**G**) The levels of expression of CD80 (**D**), CD86 (**E**), and MHC-II (**F**) by CD103⁺ DCs were analyzed. Correlation between the percentage of divided OT-I T cells (**C**) and the level of expression of CD86 on the surface of CD103⁺ DCs in the corresponding tumors (**E**) was analyzed by calculating the Pearson's correlation coefficient (**G**). Each dot represents an individual mouse and the linear regression line is shown. Cumulative data of 3 experiments (**C**–**G**) are shown (no Tregs, $n = 12$; + WT Tregs, $n = 10$; + *Prkch*$^{-/-}$ Tregs, $n = 11$). ns, $P > 0.05$; *$P \le 0.05$; **$P \le 0.01$; ***$P \le 0.001$. Statistical significance between groups was determined by 1-way ANOVA (**C**–**F**) followed by Tukey's multiple comparisons test.

which results from their impaired ability to deplete the costimulatory ligand CD86 from engaged DCs (15). To investigate whether *Prkch*$^{-/-}$ Tregs modulate APC functions in vivo, we analyzed the intratumoral DC populations in the presence of WT or *Prkch*$^{-/-}$ Tregs. Among the DCs infiltrating B16-OVA tumors, CD11c⁺MHC-II⁺ DCs can be divided in two phenotypically distinct subsets, namely CD11b⁺ and CD103⁺ DCs (Supplemental Figure 6A). As compared with mice receiving no Tregs, there was no difference in the proportion of CD11b⁺ or CD103⁺ DCs in the presence of WT or *Prkch*$^{-/-}$ Tregs (Supplemental Figure 6, B and C). Given reports that Tregs can deplete the costimulatory molecules CD80 and CD86 from engaged DCs, including in the TME (26, 27), we analyzed the expression levels of these molecules on the CD103⁺ (Figure 4, D–F) and the CD11b⁺ (Supplemental Figure 6, D–H) intratumoral DC subsets. Although the presence of WT Tregs did not affect CD103⁺ DC expression of CD80 (Figure 4D) by comparison with DCs from mice that did not receive Tregs, it significantly reduced their expression of CD86 (Figure 4E). In contrast, the levels of CD86 expressed by CD103⁺ DCs was not affected in mice that received *Prkch*$^{-/-}$ Tregs when compared with mice that did not received Tregs. Consequently, we observed significantly lower levels of CD86 on CD103⁺ DCs in the presence of WT Tregs than in the presence of *Prkch*$^{-/-}$ Tregs. As a control, we also analyzed the expression of MHC-II molecules on the same DCs (Figure 4F and Supplemental Figure 6H), revealing no significant effect of Tregs, whether WT or *Prkch*$^{-/-}$, on MHC-II expression. These data suggest that, unlike WT Tregs, which can deplete CD80 and/or CD86 from DCs (13), *Prkch*$^{-/-}$ Tregs in the TME are defective in this regard, extending our previous in vitro findings (15).

Analysis of the CD11b⁺ DC population (Supplemental Figure 6, D–H) revealed that the presence of WT Tregs reduced the expression of both CD80 and CD86 as compared with the absence of Tregs, but the levels of these costimulatory molecules were not significantly different between recipients of *Prkch*$^{-/-}$ Tregs and recipients of WT Tregs. Thus, deletion of PKCη in Tregs seems to modulate mainly the activation of the CD103⁺ DC subset in vivo via depletion of CD86.

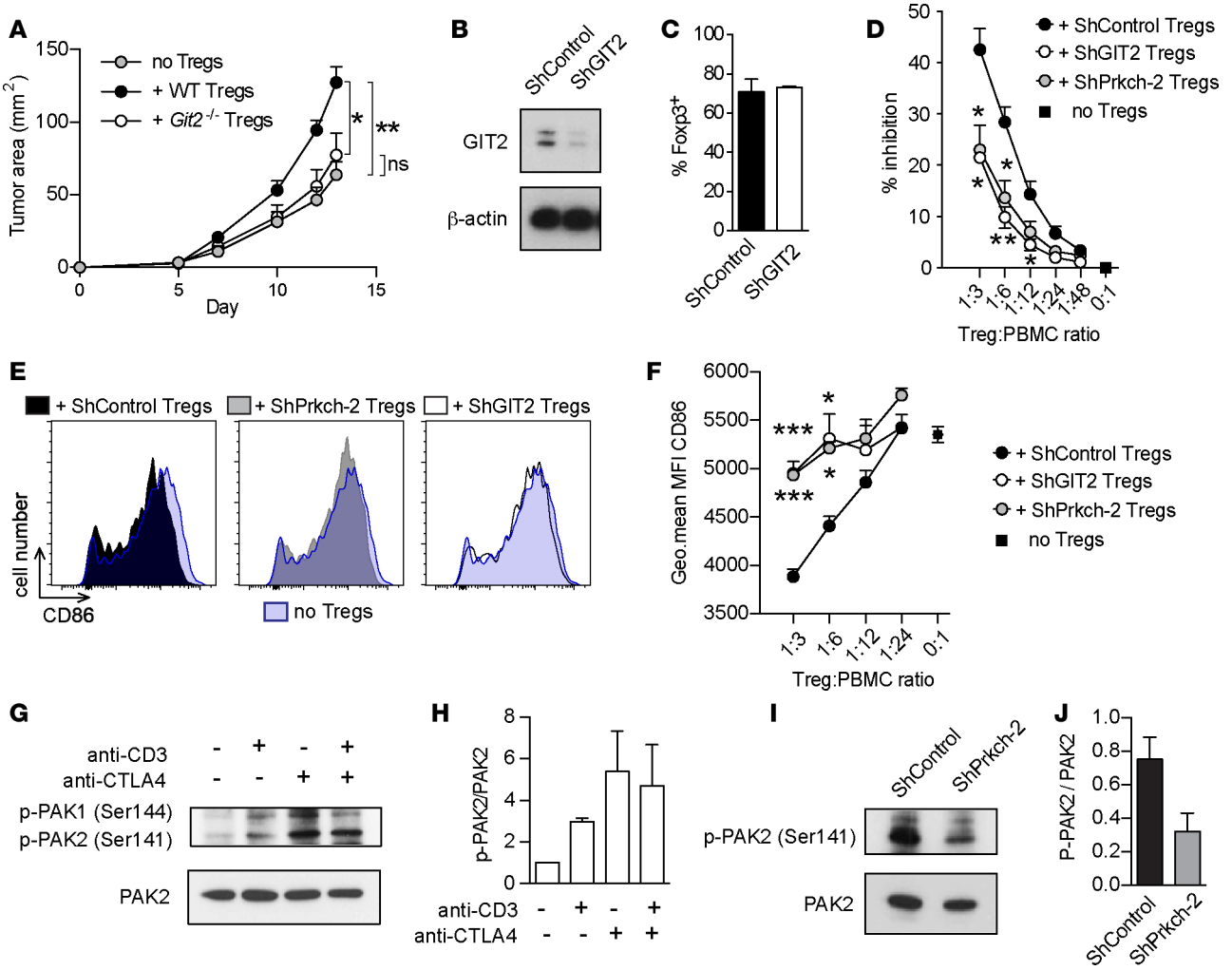

Figure 5. GIT2 controls mouse and human Treg-suppressive activity. (**A**) *Rag1*$^{-/-}$ mice received an adoptive transfer of CD25-depleted spleen cells with or without Tregs from WT or *Git2*$^{-/-}$ FIG mice and were implanted with B16-F10 melanoma cells, as in Figure 2. Tumor areas (mm^2) were measured 3 times/week. Cumulative data of 4 independent experiments are shown (mean ± SEM). no Tregs, n = 11; + WT, Tregs, n = 14; + *Prkch*$^{-/-}$ Tregs, n = 12). (**B–F**). Human Tregs were retrovirally transduced with irrelevant shRNA (ShControl) or shRNAs targeting GIT2 (shGIT2) or PKCη (ShPrkch-2). Transduced Tregs were analyzed for GIT2 protein expression by immunoblotting (**B**) and for the expression of Foxp3 by intracellular staining (**C**). Suppressive activity of transduced Tregs was evaluated by coculture with CTV-labeled PBMCs stimulated with anti-CD3 (**D**). Data are expressed as inhibition of gated CD4$^+$ Teff cell proliferation. (**E** and **F**) Analysis of CD86 expression by CD19$^+$ APCs in suppression cocultures, showing histograms of a representative mouse in each group (**E**) and cumulative data of 3 experiments (mean ± SEM) (**F**). *$P \le 0.05$; **$P \le 0.01$; ***$P \le 0.001$. Statistical significance was determined by repeated-measures 2-way ANOVA (**A**) or 1-way ANOVA (**D** and **F**) followed by Tukey's multiple comparisons test. Significance against the shControl Tregs group is shown (**D** and **F**). (**G** and **H**) Human Tregs were left unstimulated or stimulated using anti-CD3, anti-CTLA4, or a combination of both antibodies. Activating phosphorylation of PAK1 (Ser^{144}) and PAK2 (Ser^{141}) and expression levels of PAK2 were assessed in cell lysates by immunoblotting. Representative data and quantification of signals in **G** are expressed as p-PAK2/PAK2 ratio (**H**). Cumulative data from 2 experiments (mean ± SEM). (**I** and **J**) Human Tregs transduced with ShControl or ShPrkch-2 were stimulated with an anti-CTLA4 antibody. Activating phosphorylation (Ser^{141}) and total expression of PAK2 were assessed in cell lysates by immunoblotting (**I**). Signals in **I** were quantified by densitometry and expressed as p-PAK2/PAK2 ratio (**J**). Cumulative data from 2 experiments (mean ± SEM).

As CD103$^+$ DCs represent the most effective APC population that plays a key role in cross-priming antitumor CD8$^+$ T cells in the TME (24, 28), and as Treg-expressed PKCη controls both CD86 expression on these CD103$^+$ DCs (Figure 4E) and the proliferation of infiltrating OT-I CD8$^+$ T cells (Figure 4C), we analyzed the correlation between these two parameters. Interestingly, we observed a significant and positive correlation between the level of CD86 expressed by CD103$^+$ DCs and the proliferation of intratumoral OT-I T cells (Figure 4G). High levels of CD86 expressed by CD103$^+$ DCs were generally associated with increased proliferation of OT-I cells, whereas the lowest CD86 expression generally correlated with lower CD8$^+$ T cell proliferation, with intermediate levels of CD86 expression and T cell proliferation observed in the presence of *Prkch*$^{-/-}$ Tregs. Taken together, these data (Figure 4) reveal that the impaired contact-dependent suppressive activity of *Prkch*$^{-/-}$ Tregs in vivo, reflected by the reduced

ability of these Tregs to deplete costimulatory molecules, particularly CD86, from tumor-infiltrating CD103$^+$ DCs, results in increased expansion and effector function of CD8$^+$ TILs. The elevated expression of costimulatory molecules on these DCs likely supports a TME favorable for T cell priming and the development of more effective tumor-specific immunity in the presence of *Prkch*$^{-/-}$ Tregs.

GIT2 controls mouse and human Treg-suppressive activity. We previously reported that the CTLA4/PKCη signaling pathway recruits and activates the GIT/PAK/PIX pathway in mouse Tregs stimulated in vitro with anti-CD3 and anti-CTLA4 antibodies (15). This complex is required for the dissociation of focal adhesions and cellular motility in non–T cells (16, 17) and, thus, it could play a role in dissolution of the immunological synapse (IS), a specialized form of focal adhesion (29). We proposed that impaired activation of this complex in *Prkch*$^{-/-}$ Tregs may result in impaired disengagement of Tregs from DCs, accounting for the defective contact-dependent suppression of DC costimulatory function by *Prkch*$^{-/-}$ Tregs. Having demonstrated the impaired ability of *Prkch*$^{-/-}$ Tregs to control DC activation in vivo via depletion of CD80/CD86 (Figure 4), we set out to determine whether GIT2, a component of the GIT/PAK/PIX complex is also important for the ability of Tregs to inhibit an in vivo antitumor immune response. We elected to use *Git2*$^{-/-}$ mice, since they show normal T and B cell numbers in secondary lymphoid organs (30), unlike αPIX- (31, 32) and PAK2-deficient (33) mice that display impaired T cell development. We crossed *Git2*$^{-/-}$ mice (30) to FIG reporter mice to enable the identification and purification of *Git2*$^{-/-}$ GFP$^+$ Tregs. Of note, we did not observe any alterations in the number of total spleen and lymph node cells and numbers of CD4$^+$, CD8$^+$ T cells, or CD19$^+$ B cells in these mice. We then analyzed the ability of *Git2*$^{-/-}$ Tregs to inhibit the development of antitumor immune responses and promote tumor growth in vivo using the same *Rag1*$^{-/-}$ adoptive transfer system that we used before (Figure 2A) (15).

Similar to *Prkch*$^{-/-}$ Tregs (Figure 2A and Supplemental Figure 2A), *Git2*$^{-/-}$ Tregs failed to promote tumor growth by comparison with WT Tregs, and tumor growth in recipients of *Git2*$^{-/-}$ Tregs was comparable to that in mice that did not receive Tregs (Figure 5A). Thus, Treg-expressed GIT2 is required for the inhibition of antitumor immunity.

We next used a similar knockdown strategy to determine whether GIT2 is also required for the suppressive activity of human Tregs. Compared with the control shRNA, the *GIT2*-specific shRNA depleted approximately 85% of the GIT2 protein (Figure 5B) but had no effect on the proportion of Foxp3$^+$ cells (Figure 5C). In an in vitro suppression assay, the inhibition of Teff cell proliferation by Tregs was consistently lower when *GIT2* expression was knocked down and was comparable to that of *PRKCH*-knockdown Tregs (Figure 5D), indicating that GIT2 is important for the suppressive activity of human Treg.

We also investigated the effect of *PRKCH* and *GIT2* knockdown on the expression of CD86 by APCs present in the same human Treg suppression cocultures (Figure 5, E and F). We focused on CD19$^+$ B cell APCs because these cells represented the major APC population among PBMCs that we used as a source of responder T cells, and they expressed the highest levels of CD86. This analysis revealed that knockdown of either *GIT2* or *PRKCH* in human Tregs resulted in a significantly increased CD86 expression by the B cells by comparison with control shRNA-transduced Tregs. These results indicate that efficient CD86 depletion by Tregs requires not only PKCη, but also GIT2. Of interest, the decreased CD86 expression in the presence of control shRNA-transduced Tregs was particularly prominent at higher Treg/PBMC ratios (1:3 and 1:6), consistent with findings that Treg suppression is more effective at these ratios and that the degree of suppression correlates with the level of CD86 expression remaining on the APCs (34). Unlike CD86, CD80 expression by Tregs was not affected by knocking down the expression of PKCη or GIT2 (data not shown). Thus, GIT2 plays an important role as a component of the CTLA4/PKCη pathway in the suppressive activity of human Tregs via its ability to regulate the Treg/DC contact-dependent process of CD86 depletion.

Because *Git2*$^{-/-}$ mouse Tregs showed a similar impairment to that of *Prkch*$^{-/-}$ Tregs in their ability to inhibit antitumor immunity, we investigated whether PAK kinase, another component of the GIT/PIX/PAK2 pathway functions downstream of CTLA4 in human Tregs. Thus, we stimulated human Tregs with anti-CD3 and/or anti-CTLA4 antibodies and assessed the activating phosphorylation of PAK1 and PAK2 on Ser^{144} and Ser^{141}. Unstimulated human Tregs displayed weak basal phosphorylation of PAK1/2, which was enhanced by the different stimulation conditions (Figure 5, G and H). Interestingly, however, CTLA4 stimulation alone induced the maximal PAK1/2 activation compared with anti-CD3 or combined CD3 plus CTLA4 stimulation, indicating that CTLA4 engagement is sufficient to induce PAK maximal activation. To determine whether CTLA4-induced PAK2 activation in human Tregs depends on PKCη (as in

murine Tregs), we compared the activating phosphorylation of PAK2 in anti-CTLA4–stimulated human Tregs expressing shControl or shPrkch expression vectors (Figure 5, I and J). *Prkch* knockdown reduced the activating phosphorylation of PAK2, demonstrating the key role of PKCη in the activation of this signaling pathway downstream of CTLA4. Taken together, our data demonstrate that the CTLA4/PKCη/GIT/PAK/PIX signaling pathway is required for the suppressive function of both human and mouse Tregs and that disruption of this signaling axis can promote antitumor immunity.

Discussion

Tregs are a major component of the immunosuppressive TME, and they contribute to tumor escape from immune attack (35, 36). Tumor infiltration by Tregs and the resulting increase in intratumoral Treg/CD8$^+$ T cell ratios predicts poor prognosis and negatively correlates with survival in a majority of solid tumors (2, 3, 37, 38). Successful therapeutic strategies often correlate with a reduction of the number of intratumoral Tregs (39, 40). Indeed, depletion or blockade of Tregs in experimental cancer models and cancer patients can enhance tumor immunity and clearance by the immune system (41–48). Hence, there is strong interest in inhibiting or depleting Tregs in cancers (9, 49–51), but highly selective approaches to attain this objective are not yet available. The development of highly selective strategies for Treg depletion or inhibition, which minimize side effects, is further complicated by the heterogeneity of Tregs, their lack of specific surface markers, and the complex nature of their homeostatic, regulatory and effector mechanisms (52–55).

Here, we report several findings that extend our previous work (15) and provide a potentially promising approach to selectively disrupt Treg function in cancer. First, we show that, similar to our previous results using the aggressive B16-F10 melanoma (15), *Prkch*$^{-/-}$ Tregs are unable to enhance the growth of the slow growing prostate adenocarcinoma TRAMP-C1, thereby generalizing our original finding and further establishing the biological relevance of the CTLA4/PKCη pathway in the context of tumor immunity. More importantly, the current study reports several findings that provide a mechanistic basis for how deletion of PKCη in Tregs affects the development of antitumor immune responses. Second, we demonstrated directly that the presence of *Prkch*$^{-/-}$ Tregs results in enhanced numbers and proliferation of and effector cytokine expression by tumor-infiltrating CD8$^+$ (and CD4$^+$) T cells. Since we found similar numbers of WT and *Prkch*$^{-/-}$ intratumoral Tregs, we can conclude that impaired function of the *Prkch*$^{-/-}$ Tregs, rather than a reduction in their number, is responsible for the poor ability of these Tregs to inhibit antitumor Teff cell responses and, thus, enhance tumor growth. Third, we demonstrated that *Prkch*$^{-/-}$ Tregs have a defective ability to control (deplete) CD86 expression by CD103$^+$ intratumoral DCs, which correlated with increased CD8$^+$ T cell responses. Finally, we show that the GIT/PAK/PIX pathway is a critical component of the CTLA4/PKCη signaling axis that controls Treg contact-dependent suppressive function and we established the translational relevance of the CTLA4/PKCη/GIT/PAK/PIX pathway by extending our findings to human Tregs.

Among the large variety of mechanisms that Tregs can use to suppress immune responses, direct contact-dependent inhibition of the costimulatory function of APCs is prominent. Several mechanisms account for this inhibition, including depletion of APC costimulatory ligands CD80 and CD86 by transendocytosis (13), induction of inhibitory indoleamine 2,3-dioxygenase in APCs, and APC killing via TRAIL- or granzyme B–dependent mechanisms (reviewed in refs. 52, 53). Contact-dependent suppression of DC activation by Tregs also operates in the TME. For example, dynamic contacts between tumor antigen-specific Tregs and DCs resulted in reduction of CD80 expression by DCs, CD8 dysfunction, and promotion of CT26 carcinoma tumor growth (26). In another study, Treg depletion led to increased expression of CD80 and CD86 by lung DCs and enhanced antitumor T cell responses in mice bearing an advanced lung adenocarcinoma (27). These previous studies analyzed the affect of Tregs on the intratumoral CD11b$^+$ DC population, but more recent studies highlighted the essential role of the CD103$^+$CD11b$^-$ DC population in the development of effective antitumor responses: Among intratumoral DCs, the CD103$^+$ subpopulation preferentially interacts with T cells near tumor margins and exhibits unique abilities to prime naive tumor-specific CD8 T cells and stimulate activated CTLs in rodent models (24, 28). Abundance of this population in the TME also predicts outcome across human cancers (24), suggesting that this population is critical for the efficiency of immunotherapeutic strategies (24, 28). We therefore focused our analysis of intratumoral DCs in the presence of Tregs of WT or *Prkch*$^{-/-}$ origin on both the CD11b$^+$ and the CD103$^+$ DCs. In agreement with previous findings (26, 27), we found that the presence of WT Tregs reduced the expression level of CD80 and CD86 by intratumoral CD11b$^+$ DCs. We further revealed that the presence

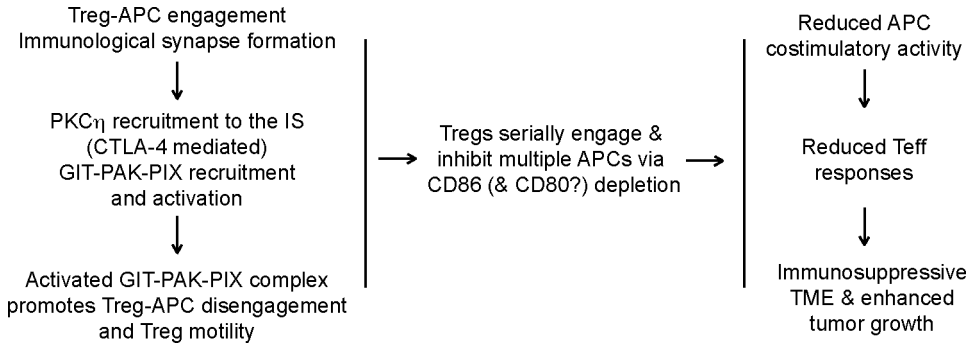

Figure 6. A model for control of Treg contact-dependent suppressive activity by PKCη. Following engagement of APCs by Tregs and formation of an immunological synapse (IS), PKCη is recruited to the Treg IS. PKCη interacts with CTLA4 in both mouse and human Tregs, and PKCη activation following CTLA4 engagement recruits and activates the GIT/PAK/PIX complex, which promotes IS disassembly and Treg motility. Activation of this complex is required for Tregs to inhibit the development of antitumor immunity in vivo and the suppressive activity of human Tregs in vitro. Efficient Treg/APC dissociation and enhanced Treg motility allow serial engagement of multiple additional APCs and depletion of their CD86 and/or CD80 costimulatory ligands by transendocytosis in a contact-dependent manner. This depletion would result in impaired APC stimulatory activity, reduced tumor-specific Teff cell responses, and, hence, promotion of tumor growth. *Prkch*$^{-/-}$ Tregs, in which the recruitment and activation of the GIT/PAK/PIX complex is impaired, are defective in serial engagement of, and depletion of CD86/CD80 from, APCs, resulting in enhanced APC stimulatory activity, a more effective Teff cell response, and reduced tumor growth. Our data implicate the CD103$^+$ DC subset as an important APC target of Treg-suppressive activity in mice.

of WT Tregs reduced the expression level of CD86 (but not CD80) by CD103$^+$ DCs, demonstrating for the first time to our knowledge the affect of Tregs on this DC subpopulation. In contrast, *Prkch*$^{-/-}$ Tregs failed to reduce the expression of CD80 and CD86 on both DC subsets, and this correlated with impaired suppressive activity and heightened numbers and effector function of infiltrating CD8$^+$ and CD4$^+$ Teff cells. These results establish a direct and positive in vivo correlation between the increased CD86 expression and a less suppressive TME reflected by the enhanced Teff cell numbers and function in the TME. Although the reason for the different effect of Tregs on CD86 versus CD80 is not clear, it is worth noting that CD86 has been considered to be the critical activating ligand via engagement of CD28 on Teff cells (56). In addition, consistent with these in vivo observations, we demonstrated previously that, following initial interaction with a first set of cocultured DCs, *Prkch*$^{-/-}$ Tregs displayed a defect in depleting CD86 from a second population of DCs added to the culture several hours later (15).

The GIT/PIX/PAK signaling pathway is a highly conserved signaling module, which controls different aspects of cytoskeletal dynamics, including cell motility and dissociation of focal adhesion across metazoans (16, 17, 57, 58). GIT binds to paxilin and PIX, thus playing a pivotal role in focal adhesion disassembly by bringing PAK (through PIX-PAK interaction) to focal adhesions (58). This complex was also found to be important for the TCR-induced activation of Jurkat T cells via its ability to promote TCR-induced activation of a key transcription factor, NFAT (59). In this study, PIX and GIT were found to promote the recruitment of PAK kinase to the T cell IS (59). Our original hypothesis linked the impaired contact-dependent suppressive activity of *Prkch*$^{-/-}$ Tregs to the impaired recruitment and activation of the GIT/PIX/PAK complex observed in the absence of PKCη (15). Our findings now provide strong experimental evidence in support of this hypothesis, as *Git2*$^{-/-}$ mouse Tregs or *GIT2*-knockdown human Tregs displayed similar functional defects to *Prkch*$^{-/-}$ Tregs in vivo (in mice) and in vitro (in humans). In the context of DC engagement by Tregs, such a defect would inhibit the dissociation of Tregs from engaged DCs, reduce Treg motility, and hinder effective serial DC engagement by motile Tregs, resulting in higher overall CD80/86 expression, more effective Teff cell stimulation, and, thus, better immune control of the tumor (Figure 6). Moreover, the ineffective serial engagement of APCs by *Prkch*$^{-/-}$ Tregs implied by our model would tilt the competition between Tregs and Teff cells for APC engagement in favor of Teff cells, thus further contributing to stronger Teff cell activation and function.

Importantly, extension of our mouse findings to human Tregs, i.e., demonstrating the relevance of the CTLA4/PKCη/GIT/PAK/PIX pathway to human Treg-suppressive functions and the control of CD86 expression by APCs, has obvious translational and clinical implications. In patients suffering from various

malignancies, alterations in the TME similar to the ones we found here in the presence of *Prkch*$^{-/-}$ Tregs correlate with better survival and response to treatment (2–6). A recent transcriptome analysis of T cell subsets purified from clinical samples of colorectal and lung tumors identified CTLA4 and PAK2 as part of a gene signature specifically upregulated in tumor-infiltrating Tregs (60). Importantly, CTLA4 and PAK2 mRNA levels were higher in tumor-infiltrating Tregs than in Tregs purified from the surrounding, nontumoral tissues or from the blood, as well as in Teff cells purified from the surrounding tissue, peripheral blood, or even from tumor-infiltrating Teff cell subsets (60). Similar observations were made for PAK2 in breast carcinoma and hepatocellular carcinoma clinical samples (61, 62). These data suggest that, in clinical situations, the CTLA4/PKCη/GIT2/PAK2/αPIX pathway plays an important and selective role in the function of intratumoral Tregs. Furthermore, our findings that this signaling axis operates in both murine and human Tregs and that knockdown of PKCη or GIT2 impaired the function of human Tregs imply that components of this pathway might represent novel valid targets of translational interest to interfere with Treg-mediated suppression in clinical settings. Hence, therapeutic targeting of the CTLA4/PKCη/GIT2/PAK2/αPIX pathway might preferentially affect intratumoral Tregs over other Treg subsets or intratumoral Teff cells. The generation and analysis of mouse models that will allow neutralization of this pathway in therapeutic settings, as monotherapy or in synergy with other modalities acting on nonredundant mechanisms, is underway.

Methods

Mice. C57BL/6 (CD45.2$^+$), *Rag1*$^{-/-}$, FIG, *Prkch*$^{-/-}$ FIG (15), *Git2*$^{-/-}$ FIG, and OT-I (CD45.1$^+$) mice were housed and maintained under specific pathogen–free conditions. *Git2*$^{-/-}$ FIG mice were generated by crossing FIG mice with *Git2*$^{-/-}$ mice (30) (gift from H. Phee, Northwestern University, Chicago, Illinois, USA). OT-I CD45.1$^+$ mice (a gift of M. von Herrath, La Jolla Institute for Allergy and Immunology) were generated by crossing the OT-I mice expressing a transgenic TCR recognizing the ovalbumin ($OVA_{257–264}$) peptide (C57BL/6-Tg(TcraTcrb)1100Mjb/J) with CD45.1$^+$ mice (B6.SJL-Ptprc^{a}Pepc^b/BoyJ). Experiments were performed in 8- to 14-week-old male or female mice; there was no gender preference, except in experiments with the TRAMP-C1 prostate carcinoma, in which only males were used.

Antibodies and reagents. Purified mAbs specific for human CD3 (OKT3), human CTLA-4 (L3D10), mouse CD3 (clone 145-2C11), and mouse CTLA-4 (clone UC10-4B9) used for stimulation were purchased from Biolegend. Fluorochrome-conjugated anti-CD45 (30-F11), anti-CD45.1 (A20), anti-CD8a (53-6.7), anti-IFN-γ (XMG1.2), anti-TNF-α (MP6-XT22), anti-PD-1 (RMP1-30), anti-Tim3 (B8.2C12), anti-Foxp3 (FJK-16s), anti-CD44 (IM7), anti-CD62L (MEL-14), anti-CD25 (PC61), anti-CD11c (N418), anti-I-A/I-E (M5/114.15.2), anti-CD11b (M1/70), anti-CD103 (2E7), anti-CD80 (16-10A1), anti-CD86 (GL-1), anti-F4-80 (BM8), and anti-Gr1 (RB6-8C5) were purchased from Biolegend. Fluorochrome-conjugated anti-CD4 (RM4-5) and anti-CD19 (1D3) and biotinylated anti-CD25 (PC61.5) were obtained from eBiosciences. The following fluorochrome-conjugated mAbs specific for human antigens were used: anti-CD4 (RPAT4) were obtained from TONBO and anti-CD8 (RPAT8), anti-Foxp3 (206D), anti-CD19 (HIB19), and anti-CD86 (IT2.2) were purchased from Biolegend. 7-AAD (BD Biosciences) or Fixable Viability Dye (eBioscience) were used to exclude dead cells in flow cytometry samples, and the CTV Cell Proliferation Kit (Life Technologies) was used to analyze cell division. For immunoblotting, anti-PKCη (C-15) and anti-β-actin (C4) were obtained from Santa Cruz Biotechnology; anti-PAK2, anti-GIT2 (D11B8), and anti-phospho-PAK1 (Ser144)/PAK2 (Ser141) were obtained from Cell Signaling; and horseradish peroxidase–conjugated anti-rabbit IgG (from donkey) and anti-mouse IgG (from sheep) were obtained from GE Healthcare.

Immunoprecipitation and immunoblotting. Cell lysates were prepared in 1% NP-40 lysis buffer (50 mM Tris-HCl, pH 7.5, 50 mM NaCl, and 5 mM EDTA). For immunoprecipitation, lysates were incubated with primary antibodies (3 μg), followed by overnight incubation with protein G-Sepharose beads (GE healthcare) and centrifugation. Proteins were separated on sodium dodecyl sulfate–polyacrylamide gels under reducing conditions and transferred onto PVDF membranes (EMB Millipore) for immunoblotting analysis. Membranes were treated with primary antibodies, followed by incubation with horseradish peroxidase–conjugated secondary antibodies, and signal was visualized using the ECL luminescence system (Amersham Biosciences). Signal intensities were quantified using ImageJ software (NIH).

Cell purification. For use as a source of effector cells for adoptive transfer into *Rag1*$^{-/-}$ mice, C57BL/6 spleen cell suspensions were depleted of CD25$^+$ cells using biotinylated anti-CD25 mAb and streptavidin-conjugated magnetic beads for negative selection on LS columns (Miltenyi). Tregs from WT, *Prkch*$^{-/-}$,

and *Git2*$^{-/-}$ FIG mice were obtained by first purifying CD4$^+$ T cells by negative selection (Miltenyi) and then sorting GFP$^+$ Tregs on a FACSAria-II sorter (BD Biosciences). OT-I CD8$^+$ T cells used for adoptive transfer in B16-OVA tumor-bearing recipients were isolated from the spleens of OT-I CD45.1$^+$ naive mice by immunomagnetic negative selection (Stemcell). Human PBMCs were isolated by centrifugation on Histopaque-1077 gradient (MilliporeSigma) and frozen for later use as responder T cells or directly used to purify CD4$^+$CD25$^+$CD127^{lo} Tregs by immunomagnetic negative selection (StemCell).

Tumor models and adoptive transfers. B16-F10 and TRAMP-C1 tumor cell lines were obtained from ATCC, passaged twice, and tested negative for mycoplasma. The OVA-transfected B16 melanoma tumor cell line (B16-OVA) (gift from S. Schoenberger, La Jolla Institute for Allergy and Immunology) tested negative for mycoplasma and was authenticated using STR and MAPP testing. All culture media were supplemented with 10% FBS, with 10% heat-inactivated FBS, 2 mM glutamine, 1 mM sodium pyruvate, 1 mM MEM nonessential amino acids, and 100 U/ml each of penicillin and streptomycin (Life Technologies). B16 tumor cell lines were cultured in Iscove's modified Dulbecco's medium, and the TRAMP-C1 tumor cell line was cultured in Dulbecco's Modified Eagle's Medium in the presence of bovine insulin (5 μg/ml; MilliporeSigma) and dehydroisoandrosterone (10 nM; MilliporeSigma). Cells were harvested for injection by a brief incubation with trypsin followed by mechanical treatment. For in vivo tumor experiments, *Rag1*$^{-/-}$ recipients were adoptively transferred with 15×10^6 CD25-depleted spleen cells alone or together with 0.5×10^6 GFP$^+$ Tregs (from WT, *Prkch*$^{-/-}$, or *Git2*$^{-/-}$ FIG mice). On the next day, B16-F10 (5×10^5 cells, i.d. injection) or TRAMP-C1 tumor cells (5×10^6, s.c. injection) were inoculated on the flank. Tumor length and width were measured 3 times/week using an electronic digital caliper to calculate tumor area (length × width). When indicated, 3×10^6 CTV-labeled naive OT-I CD45.1$^+$CD8 T cells were injected i.v. in B16-OVA tumor-bearing mice 10 days after tumor injection.

TME analysis and in vitro restimulation. At experiment endpoint (day 40 for TRAMP-C1 tumors and day 14 for B16-F10 melanoma), the following methods were used to generate single-cell suspensions from tumors: TRAMP-C1 tumors were cut in small pieces and dissociated into single-cell suspensions using the gentleMACS Octo Dissociator (Miltenyi) and the mouse tumor dissociation kit (Miltenyi) according to the manufacturer's instructions. B16 tumors were cut in small pieces and digested for 15 minutes at 37°C in RPMI media containing TL Liberase (100 μg/ml; Roche) and DNAseI (200 μg/ml; MilliporeSigma). Then, TL Liberase was added to reach a final concentration of 150 μg/ml for an additional 10-minute incubation. Tumor cell suspensions were subjected to red blood cell lysis, passed through 40-μm cell strainers, and washed with PBS/2% FBS/2 mM EDTA before use. For cytokine analysis upon ex vivo restimulation, whole tumor cell suspensions were plated in RPMI media containing PMA (50 ng/ml), ionomycin (1 μM), and Golgiplug (BD Biosciences) for 4 hours at 37°C. Intracellular staining was performed using the Cytofix/Cytoperm kit (BD Biosciences). Data were acquired on LSR-II cytometers (Becton Dickinson) and analyzed using FlowJo software (Tree Star).

Plasmids and lentiviral particles production. shRNAs targeting human *PRKCH* or human *GIT2* designed by The RNAi Consortium were obtained from GE Dharmacon in the pLKO.1 lentiviral vector containing a puromycin selection cassette. The original pLKO.1-puro vectors were modified to replace the puromycin resistance gene by a fluorescent reporter gene (GFP or Ametrine). HEK293T cells (6×10^5 per well in 6-well plate) were transfected with a mixture of the following plasmid DNAs for virion production: pMDGLg/pRRE (Addgene 12251, 1 μg), pRSV-rev (Addgene 12253, 1 μg), pMD2.G (Addgene 12259, 1 μg), pLKO.1-shRNA (2 μg) plasmid DNA. 15 μl TransIT-LT1 (Mirus) transfection reagent was used per well. After overnight incubation, the media were replaced and culture supernatants were obtained after an additional 24 hours of culture were used to infect in vitro–activated Tregs.

Human Treg in vitro expansion. Purified CD4$^+$CD25$^+$CD127^{lo} Tregs were expanded in X-vivo 15 medium supplemented with 10% AB Serum (Valley Biomedical) penicillin-streptomycin (100 U/ml; Life Technologies), Glutamine (2 mM; Life Technologies), and MEM nonessential amino acids (1 mM; Life Technologies). 5×10^5 Tregs cells were stimulated with anti-CD3/anti-CD28–coated microbeads (Invitrogen) at a 1:1 bead-to-cell ratio in 24-well plates. After 24 hours, recombinant human IL-2 was added to the cultures (300 U/ml; Peprotech). Fresh media containing IL-2 was added on day 4, and cultures were diluted on days 5 and 7. Aliquots of expanded Tregs were frozen on day 9 for further use.

Human Treg transduction and Treg suppression assay. 5×10^5 Tregs were stimulated in 24-well plates with anti-CD3 plus anti-CD28-coated microbeads (Life Technologies Inc.) at a 1:1 bead-to-cell ratio in X-vivo 15 media containing IL-2 (300 U/ml). After 24 hours, 500 μl culture media was removed and replaced with

freshly collected supernatants containing lentiviral particles. Supernatants were supplemented in polybrene (MilliporeSigma) to achieve a final concentration of 5 μg/ml. Infection was performed by centrifugation at 805 *g* for 60 minutes at 37°C. Fresh media containing IL-2 was added to the wells after 24 hours, and transduced Tregs (GFP^+ or $Ametrine^+$) were purified by cell sorting after 5 days. Transduced Tregs were then rested in the absence of CD3/CD28 stimulation but in the presence of IL-2 for 4 additional days. Before use for suppressive assay, shRNA-expressing Tregs and freshly thawed PBMCs were rested overnight in the absence of stimulation or IL-2. For the Treg suppression assay, 1.5×10^5 CTV-labeled PBMCs were stimulated in anti-CD3–coated (0.3 μg/ml) flat-bottom 96-well plates in the presence of various numbers of Tregs in RPMI medium. After 4 days, cell division of responder T cells is assessed by flow cytometry by gating on the $CD4^+CTV^+$ T cell population. Data are expressed as percentage of inhibition, calculated by comparing the percentage of responder cells divided at least once in Treg-containing wells to the percentage of divided responder cells stimulated in the absence of Tregs. For analysis of CD86 expression by $CD19^+$ B cells, analysis was conducted on day 3.

Statistics. When 3 groups were compared, analysis of statistical significance was determined by ANOVA and Tukey's multiple comparisons test. One-way ANOVA was used when the analysis was performed at a single time point, and repeated-measures 2-way ANOVA was used for analysis of tumor growth experiments. When only 2 groups were compared, 2-tailed unpaired *t* test was used. *P* values of less than 0.05 were considered significant.

Study approval. All animal studies were approved by the La Jolla Institute for Allergy and Immunology Animal Care Committee. Human blood samples were obtained from healthy donors through the La Jolla Institute for Allergy and Immunology Clinical Core in accordance with the La Jolla Institute for Allergy and Immunology Normal Blood Donor Program (VD-057).

Author contributions

CP and AJCB conducted experiments, collected data, and performed analyses. CP, KFK, and AA designed the study and wrote the paper.

Acknowledgments

We thank members of the Altman laboratory for discussions, especially Marjorie Cote for critical advice on shRNA-mediated knockdown; the Flow Cytometry Core Unit and the Animal Husbandry Unit of the La Jolla Institute for Allergy and Immunology for excellent services; and Hyewon Phee for providing the *Git2*$^{-/-}$ mice. This is publication number 3043 from the La Jolla Institute for Allergy and Immunology. CP is a Cancer Research Institute Irvington Fellow supported by the Cancer Research Institute.

Address correspondence to: Amnon Altman, 9420 Athena Circle, La Jolla, California 92037, USA. Phone: 858.752.6808; Email: amnon@lji.org. Or to: Kok-Fai Kong, 10724 Science Center Drive, San Diego, California 92121, USA. Phone: 858.622.7482; Email: Kok-Fai.Kong@pfizer.com.

1. Schreiber RD, Old LJ, Smyth MJ. Cancer immunoediting: integrating immunity's roles in cancer suppression and promotion. *Science*. 2011;331(6024):1565–1570.
2. Sato E, et al. Intraepithelial CD8+ tumor-infiltrating lymphocytes and a high CD8+/regulatory T cell ratio are associated with favorable prognosis in ovarian cancer. *Proc Natl Acad Sci USA*. 2005;102(51):18538–18543.
3. Gao Q, et al. Intratumoral balance of regulatory and cytotoxic T cells is associated with prognosis of hepatocellular carcinoma after resection. *J Clin Oncol*. 2007;25(18):2586–2593.
4. Fridman WH, Pagès F, Sautès-Fridman C, Galon J. The immune contexture in human tumours: impact on clinical outcome. *Nat Rev Cancer*. 2012;12(4):298–306.
5. Galon J, et al. Towards the introduction of the 'Immunoscore' in the classification of malignant tumours. *J Pathol*. 2014;232(2):199–209.
6. Mlecnik B, et al. Integrative analyses of colorectal cancer show immunoscore is a stronger predictor of patient survival than microsatellite instability. *Immunity*. 2016;44(3):698–711.
7. Topalian SL, Drake CG, Pardoll DM. Immune checkpoint blockade: a common denominator approach to cancer therapy. *Cancer Cell*. 2015;27(4):450–461.
8. Lonberg N, Korman AJ. Masterful antibodies: Checkpoint blockade. *Cancer Immunol Res*. 2017;5(4):275–281.
9. Liu C, Workman CJ, Vignali DA. Targeting regulatory T cells in tumors. *FEBS J*. 2016;283(14):2731–2748.
10. Hodi FS, et al. Improved survival with ipilimumab in patients with metastatic melanoma. *N Engl J Med*. 2010;363(8):711–723.
11. Walker LS, Sansom DM. The emerging role of CTLA4 as a cell-extrinsic regulator of T cell responses. *Nat Rev Immunol*. 2011;11(12):852–863.

12. Wing K, et al. CTLA-4 control over Foxp3+ regulatory T cell function. *Science*. 2008;322(5899):271–275.
13. Qureshi OS, et al. Trans-endocytosis of CD80 and CD86: a molecular basis for the cell-extrinsic function of CTLA-4. *Science*. 2011;332(6029):600–603.
14. De Velasco G, et al. Comprehensive meta-analysis of key immune-related adverse events from CTLA-4 and PD-1/PD-L1 inhibitors in cancer patients. *Cancer Immunol Res*. 2017;5(4):312–318.
15. Kong KF, et al. Protein kinase C-η controls CTLA-4-mediated regulatory T cell function. *Nat Immunol*. 2014;15(5):465–472.
16. Zhao ZS, Manser E, Loo TH, Lim L. Coupling of PAK-interacting exchange factor PIX to GIT1 promotes focal complex disassembly. *Mol Cell Biol*. 2000;20(17):6354–6363.
17. Lucanic M, Cheng HJ. A RAC/CDC-42-independent GIT/PIX/PAK signaling pathway mediates cell migration in C. elegans. *PLoS Genet*. 2008;4(11):e1000269.
18. Ahmadzadeh M, et al. Tumor antigen-specific CD8 T cells infiltrating the tumor express high levels of PD-1 and are functionally impaired. *Blood*. 2009;114(8):1537–1544.
19. Sakuishi K, Apetoh L, Sullivan JM, Blazar BR, Kuchroo VK, Anderson AC. Targeting Tim-3 and PD-1 pathways to reverse T cell exhaustion and restore anti-tumor immunity. *J Exp Med*. 2010;207(10):2187–2194.
20. Jiang Y, Li Y, Zhu B. T-cell exhaustion in the tumor microenvironment. *Cell Death Dis*. 2015;6:e1792.
21. Penaloza-MacMaster P, et al. Interplay between regulatory T cells and PD-1 in modulating T cell exhaustion and viral control during chronic LCMV infection. *J Exp Med*. 2014;211(9):1905–1918.
22. Wherry EJ, Kurachi M. Molecular and cellular insights into T cell exhaustion. *Nat Rev Immunol*. 2015;15(8):486–499.
23. Fourcade J, et al. Upregulation of Tim-3 and PD-1 expression is associated with tumor antigen-specific CD8+ T cell dysfunction in melanoma patients. *J Exp Med*. 2010;207(10):2175–2186.
24. Broz ML, et al. Dissecting the tumor myeloid compartment reveals rare activating antigen-presenting cells critical for T cell immunity. *Cancer Cell*. 2014;26(5):638–652.
25. Broz ML, Krummel MF. The emerging understanding of myeloid cells as partners and targets in tumor rejection. *Cancer Immunol Res*. 2015;3(4):313–319.
26. Bauer CA, Kim EY, Marangoni F, Carrizosa E, Claudio NM, Mempel TR. Dynamic Treg interactions with intratumoral APCs promote local CTL dysfunction. *J Clin Invest*. 2014;124(6):2425–2440.
27. Joshi NS, et al. Regulatory T cells in tumor-associated tertiary lymphoid structures suppress anti-tumor t cell responses. *Immunity*. 2015;43(3):579–590.
28. Salmon H, et al. Expansion and activation of CD103(+) dendritic cell progenitors at the tumor site enhances tumor responses to therapeutic PD-L1 and BRAF inhibition. *Immunity*. 2016;44(4):924–938.
29. Wehrle-Haller B. Structure and function of focal adhesions. *Curr Opin Cell Biol*. 2012;24(1):116–124.
30. Phee H, et al. Regulation of thymocyte positive selection and motility by GIT2. *Nat Immunol*. 2010;11(6):503–511.
31. Missy K, et al. AlphaPIX Rho GTPase guanine nucleotide exchange factor regulates lymphocyte functions and antigen receptor signaling. *Mol Cell Biol*. 2008;28(11):3776–3789.
32. Korthals M, et al. αPIX RhoGEF supports positive selection by restraining migration and promoting arrest of thymocytes. *J Immunol*. 2014;192(7):3228–3238.
33. Phee H, et al. Pak2 is required for actin cytoskeleton remodeling, TCR signaling, and normal thymocyte development and maturation. *Elife*. 2014;3:e02270.
34. Hou TZ, et al. A transendocytosis model of CTLA-4 function predicts its suppressive behavior on regulatory T cells. *J Immunol*. 2015;194(5):2148–2159.
35. Gajewski TF, et al. Cancer immunotherapy strategies based on overcoming barriers within the tumor microenvironment. *Curr Opin Immunol*. 2013;25(2):268–276.
36. Pitt JM, et al. Resistance mechanisms to immune-checkpoint blockade in cancer: Tumor-intrinsic and -extrinsic factors. *Immunity*. 2016;44(6):1255–1269.
37. Shang B, Liu Y, Jiang SJ, Liu Y. Prognostic value of tumor-infiltrating FoxP3+ regulatory T cells in cancers: a systematic review and meta-analysis. *Sci Rep*. 2015;5:15179.
38. Saito T, et al. Two FOXP3(+)CD4(+) T cell subpopulations distinctly control the prognosis of colorectal cancers. *Nat Med*. 2016;22(6):679–684.
39. Selby MJ, et al. Anti-CTLA-4 antibodies of IgG2a isotype enhance antitumor activity through reduction of intratumoral regulatory T cells. *Cancer Immunol Res*. 2013;1(1):32–42.
40. Steinberg SM, et al. BRAF inhibition alleviates immune suppression in murine autochthonous melanoma. *Cancer Immunol Res*. 2014;2(11):1044–1050.
41. Shimizu J, Yamazaki S, Sakaguchi S. Induction of tumor immunity by removing CD25+CD4+ T cells: a common basis between tumor immunity and autoimmunity. *J Immunol*. 1999;163(10):5211–5218.
42. Onizuka S, Tawara I, Shimizu J, Sakaguchi S, Fujita T, Nakayama E. Tumor rejection by in vivo administration of anti-CD25 (interleukin-2 receptor alpha) monoclonal antibody. *Cancer Res*. 1999;59(13):3128–3133.
43. Bui JD, Uppaluri R, Hsieh CS, Schreiber RD. Comparative analysis of regulatory and effector T cells in progressively growing versus rejecting tumors of similar origins. *Cancer Res*. 2006;66(14):7301–7309.
44. Rech AJ, et al. CD25 blockade depletes and selectively reprograms regulatory T cells in concert with immunotherapy in cancer patients. *Sci Transl Med*. 2012;4(134):134ra62.
45. Pere H, et al. A CCR4 antagonist combined with vaccines induces antigen-specific CD8+ T cells and tumor immunity against self antigens. *Blood*. 2011;118(18):4853–4862.
46. Sugiyama D, et al. Anti-CCR4 mAb selectively depletes effector-type FoxP3+CD4+ regulatory T cells, evoking antitumor immune responses in humans. *Proc Natl Acad Sci USA*. 2013;110(44):17945–17950.
47. Dannull J, et al. Enhancement of vaccine-mediated antitumor immunity in cancer patients after depletion of regulatory T cells. *J Clin Invest*. 2005;115(12):3623–3633.
48. Kurose K, et al. Phase Ia study of FoxP3+ CD4 Treg depletion by infusion of a humanized anti-CCR4 antibody, KW-0761, in cancer patients. *Clin Cancer Res*. 2015;21(19):4327–4336.

49. Pere H, et al. Comprehensive analysis of current approaches to inhibit regulatory T cells in cancer. *Oncoimmunology*. 2012;1(3):326–333.
50. Takeuchi Y, Nishikawa H. Roles of regulatory T cells in cancer immunity. *Int Immunol*. 2016;28(8):401–409.
51. Tanaka A, Sakaguchi S. Regulatory T cells in cancer immunotherapy. *Cell Res*. 2017;27(1):109–118.
52. Vignali DA, Collison LW, Workman CJ. How regulatory T cells work. *Nat Rev Immunol*. 2008;8(7):523–532.
53. Tang Q, Bluestone JA. The Foxp3+ regulatory T cell: a jack of all trades, master of regulation. *Nat Immunol*. 2008;9(3):239–244.
54. Barbi J, Pardoll D, Pan F. Treg functional stability and its responsiveness to the microenvironment. *Immunol Rev*. 2014;259(1):115–139.
55. Campbell DJ. Control of regulatory T cell migration, function, and homeostasis. *J Immunol*. 2015;195(6):2507–2513.
56. Sansom DM, Manzotti CN, Zheng Y. What's the difference between CD80 and CD86? *Trends Immunol*. 2003;24(6):314–319.
57. Manabe R, Kovalenko M, Webb DJ, Horwitz AR. GIT1 functions in a motile, multi-molecular signaling complex that regulates protrusive activity and cell migration. *J Cell Sci*. 2002;115(Pt 7):1497–1510.
58. Hoefen RJ, Berk BC. The multifunctional GIT family of proteins. *J Cell Sci*. 2006;119(Pt 8):1469–1475.
59. Phee H, Abraham RT, Weiss A. Dynamic recruitment of PAK1 to the immunological synapse is mediated by PIX independently of SLP-76 and Vav1. *Nat Immunol*. 2005;6(6):608–617.
60. De Simone M, et al. Transcriptional landscape of human tissue lymphocytes unveils uniqueness of tumor-infiltrating T regulatory cells. *Immunity*. 2016;45(5):1135–1147.
61. Plitas G, et al. Regulatory T cells exhibit distinct features in human breast cancer. *Immunity*. 2016;45(5):1122–1134.
62. Zheng C, et al. Landscape of infiltrating T cells in liver cancer revealed by single-cell sequencing. *Cell*. 2017;169(7):1342–1356.e16.